ACS OMEGA

http://pubs.acs.org/journal/acsodf

Article

# Effect of Carbonate Source on the Dehydrofluorination Process in Polyvinylidene Fluoride/Alkali Metal Carbonate Composites

Wenliang Zhu,* Kohei Okada, Naoki Hoshida, Yumi Yoshida, Alessandro Martucci, Jiliang Zhu,* Elia Marin, and Giuseppe Pezzotti

Cite This: *ACS Omega* 2023, 8, 14944−14951

Read Online

ACCESS | Metrics & More | Article Recommendations | Supporting Information

**ABSTRACT:** In this paper, Raman and X-ray photoelectron spectroscopies were applied to analyze compositional and structural variations of the generated activated carbon (AC), as induced by changing carbonate source in three different types of systems, PVDF/$M_2CO_3$ (M = Li, Na, and K). According to the variations of $I_D/I_G$ and $sp^2/sp^3$ ratios, a strong dependence of the AC structure on the type and content of the initial carbonate was found, determined by practical dehydrofluorination reactions associated with oxygen incorporation in AC and side reactions, because of the property variation induced by the difference in the cation of the carbonate sources. This procedure clarified the process of PVDF dehydrofluorination and the formation of activated carbon, which helps to optimize the material performance of the percolative composite for flexible energy storage applications.

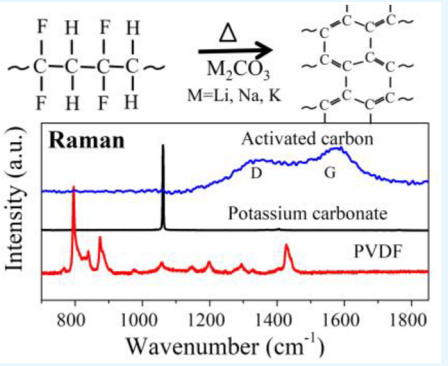


## 1. INTRODUCTION

In recent years, polyvinylidene fluoride (PVDF)-based ceramic−polymer composites have attracted intensive attention for flexible energy storage/electronics applications, taking advantage of its high flexibility, low mechanical impedance, and low dielectric loss.[1−3] For composites with conductive and dielectric phases, inner microcapacitors can be formed in a series along an external field, in which the conductive phases act as electrodes and the dielectric phases are insulating media.[1] In a previous paper, we have reported that percolative composites consisting of potassium carbonate dispersed in polyvinylidene fluoride (PVDF) polymeric matrix showed a rather high dielectric constant and electrical conductivity at the percolation threshold (30 wt % $K_2CO_3$) due to the formation of chemically activated interfaces in the composite,[4] as interfacial polarization resulted in high values of dielectric permittivity.[5] Further studies revealed the presence of a complex reaction loop for the formation of activated carbon (AC) from PVDF dehydrofluorination during thermal treatment, as the net effect of these reactions is to generate a carbon-based nanocomposite in the polymer matrix.[6,7] The system has many marked merits: e.g., low-cost raw materials, extremely simple fabrication procedure, mesoporous surface structure, high flexibility, and light weight, which makes it promising for portable, flexible, and wearable energy storage applications.

However, the system encountered problems of significant alteration of microstructure and material property with the fabrication process because of the occurrence of complex and uncontrolled reactions during thermal treatments.[6] Accordingly, further evaluation of the reactions that occur upon thermal treatments is needed for clarifying the formation mechanism of activated carbon and its detailed structure. In addition, the variation of the carbonate source may exert a significant influence on the dehydrofluorination reactions and thus the final properties of activated carbon, because of the distinct properties of the carbonates caused by the difference in the cations. For instance, it has been reported that ZnO films doped with various alkaline metal carbonates showed quite different electron mobilities and work functions, which could lead to different electron injection properties of these devices and differences in the device performance.[8,9] Moreover, the incorporation of ion-rich materials in the composite can provide faster ion transport when the composite is charged.[10] In particular, smaller ions can easily disperse to be adsorbed in the nanopores of AC and contribute to increasing the charging and discharging rates of the electrode.

Accordingly, in this study, we attempted to compare different types of PVDF-based composite systems fabricated from mixtures of PVDF and different alkali metal carbonates, PVDF/$M_2CO_3$ (M = Li, Na, and K), aiming at clarifying the influence of carbonate source on the process of PVDF dehydrofluorination according to an analysis of the structure

**Received:** October 26, 2022
**Accepted:** February 14, 2023
**Published:** April 18, 2023

of generated activated carbon under different experimental conditions. Since the degree of $sp^2$ hybridizations (or the $sp^2/sp^3$ ratio) in the samples plays a critical role in material performance,[11−14] the chemical composition and structure of the products were analyzed by Raman and X-ray photoelectron spectroscopies (XPS). The results revealed a strong dependence of the structure of AC on the type and content of the initial carbonate source. Clarifying these issues will provide the foundation for applying the percolative composite to flexible energy storage systems.

## 2. EXPERIMENTS

The investigated percolative samples were fabricated by a low-temperature thermal treatment in the air of mixtures of PVDF and $M_2CO_3$. The raw powders of $M_2CO_3$ (Nacalai Tesque) and PVDF (Apollo Scientific Ltd., 0.1 g) were mixed by ball milling with ethanol at different mass fractions of $M_2CO_3$ (20, 30, and 40 wt %), separately, and then dissolved by *N*,*N*-dimethylformamide to form a gelled solution at 60 °C by constant stirring. After that, the gelled solutions were deposited on an aluminum foil and underwent thermal treatments at 220 °C for 1 h. More details about the fabrication procedure can be found in our previous paper.[6] Accordingly, the obtained film samples were denoted as PLC for PVDF/$Li_2CO_3$, PNC for PVDF/$Na_2CO_3$, and PKC for PVDF/$K_2CO_3$. For comparison, a pure PVDF sample without mixing with $M_2CO_3$ was also thermally treated under the same conditions.

Raman spectra of the samples were collected at room temperature using a confocal optical microprobe and a single monochromator (T-64000, Jobin-Ivon/Horiba Group, Kyoto, Japan). The 514.5 nm green line of an Ar-ion laser was used as the excitation source. An average of 20 spectra collected at different locations for each sample were analyzed here, and spectral deconvolution was performed by means of commercially available software (LabSpec, Horiba/Jobin-Yvon, Kyoto, Japan).

XPS analyses were performed at three different locations for each sample by using a photoelectron spectrometer (JPS-9010 MC; JEOL Ltd., Tokyo, Japan) with an X-ray source of monochromatic Mg K$\alpha$ (output 10 kV, 10 mA). A single crystalline silicon piece (core-level line 99.4 eV, Si 2p) was used to calibrate the scale of the binding energies. Since all samples were stored under the same conditions, the influence of possibly existent adventitious carbon[15] on the observed variations of composition fractions among the samples could be neglected.

## 3. RESULTS

Figure 1 shows the average Raman spectra of the PLC, PNC, and PKC samples with carbonate content of 30 wt %. All of these samples exhibit typical D (~1350 $cm^{-1}$) and G (~1580 $cm^{-1}$) peaks of carbon peculiar to a graphitized ringlike structure, while none of the Raman bands from the raw materials could be observed after thermal treatments. The D peak of carbon is known to arise from a defected/disordered graphitic structure [this breathing mode ($A_{1g}$) is Raman inactive in $sp^2$ graphite], while the G peak originates from bond stretching of all pairs of $sp^2$ atoms in both rings and chains (i.e., the zone center $E_{2g}$ mode in the case of graphite).[16] The Raman spectra of pure PVDF showed an insignificant variation after thermal treatments at the same conditions, as no D or G bands were observed. In general, the

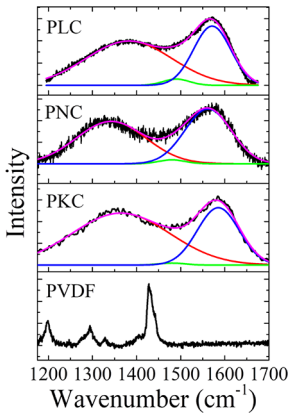


**Figure 1.** Typical Raman spectra of the investigated PLC, PNC, and PKC samples and the raw material, PVDF, subjected to thermal treatments.

PNC samples exhibited weaker signals of D and G bands than the other samples under the same measurement conditions. According to our previous study,[6] spectral deconvolution could be performed using Gaussian functions, which revealed the presence of D and G peaks and a C−H bending-induced small sub-band located at around 1480 $cm^{-1}$ (cf. fitting curves shown in Figure 1). The values of the ratio, $I_D/I_G$, for the samples were calculated using the areas under the respective deconvoluted bands. Note that, according to the three-stage model proposed to characterize disordered/amorphous carbon phases,[16,17] the intensity ratio of D and G peaks has been taken to be associated with the $sp^2$ content of graphitelike carbon: the ratio of $I_D/I_G$ increases with increasing $sp^2$ content for the formation of nanocrystalline graphite.

Accordingly, the variation of $I_D/I_G$ for all of the investigated samples could be obtained after respective spectral deconvolution, as shown by the results in Figure 2. As can be seen, the

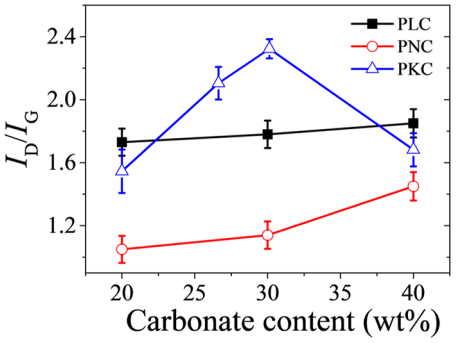


**Figure 2.** Variations of $I_D/I_G$ with carbonate content for the investigated PLC, PNC, and PKC samples.

PNC samples showed smaller $I_D/I_G$ values than the others. Increasing carbonate content resulted in a different increase of $I_D/I_G$ for both PLC and PNC, unlike PKC, which showed a significant increase of $I_D/I_G$ from ~1.6 (at 20 wt %) to a maximum value of around 2.4 at the carbonate content of 30 wt % and subsequently a decrease to ~1.6 (at 40 wt %).[6]

To further investigate chemical and compositional variations in the samples, XPS analyses were carried out on the samples, as a comparison of collected high-resolution C 1s XPS spectra for the investigated PLC, PNC, and PKC samples with 30 wt % carbonate shown in Figure 3. The C 1s XPS spectra revealed


https://doi.org/10.1021/acsomega.2c06857
ACS Omega 2023, 8, 14944−14951

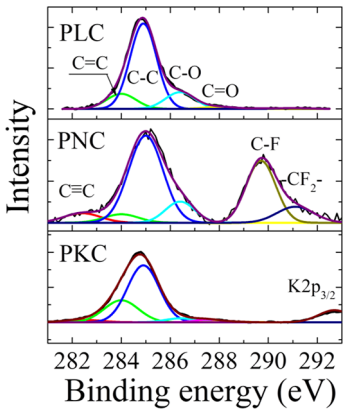


**Figure 3.** C 1s XPS spectra of the investigated PLC, PNC, and PKC samples.

the presence of broad and asymmetric bands in the range from 281 to 293 eV for the samples, which could be deconvoluted into at least four peaks, assigned to C═C (284 eV), C—C (285 eV), C—O (286.5 eV), and C═O (287.5 eV),[6,18] respectively. However, in the case of PNC, a lower energy shoulder located at around 282.5 eV could be observed, which was taken to be attributed to alkyne (C≡C), as will be discussed in the following section. A broad band located at ∼290 eV also appeared, contributed by the sub-bands of C—F (289.5 eV) and C—$F_2$ (291 eV).[4] The C—F-related bands, which were clearly observable in the mixed and untreated PKC sample (prepared at room temperature), could hardly be observed in PLC and PKC after thermal treatment. According to spectral deconvolution, the fraction of each sub-band in the samples could be determined from respective peak areas.

Accordingly, the variations of the ratio of $sp^2$ (C═C) to $sp^3$ (C—C) carbon fractions, $sp^2/sp^3$, and the oxygen-related fraction (sum of the fractions of C—O and C═O in the C 1s XPS spectrum) with carbonate content for the investigated PLC, PNC, and PKC samples could be obtained and are shown in Figure 4. As can be seen, similar to the cases of $I_D/I_G$ variation, the PNC samples showed smaller $sp^2/sp^3$ than PLC and PKC, and unlike PKC that showed a maximum value at 30 wt %, both PLC and PNC exhibited a different increase of $sp^2/sp^3$ with increasing carbonate content. In general, the PLC samples showed a higher oxygen-related content than PNC and PKC.

Figures 5 and 6 show high-resolution XPS spectra of O 1s and F 1s for the investigated PLC, PNC, and PKC samples, respectively. The O 1s XPS spectra exhibit four peaks assigned to Li—O (529.5 eV) (Na—O, 529.8 eV; K—O, 530.2 eV), C═O (∼531.2 eV), C—O (∼532.5 eV), and O—H (534.0 eV). In most of the PLC samples, the Li—O peak has almost completely disappeared, indicating that the raw material $Li_2CO_3$ was fully consumed for the reactions, similar to PKC, while in the cases of PNC, the fractions of Na—O and C═O occupied a relatively high percent. A relatively high fraction of OH could be found in the PLC samples, despite an insignificant change with increasing carbonate content.

The F 1s XPS spectra of the PLC and PKC samples exhibit two peaks assigned to Li−F (K−F) and H−F; however, for PNC, a dominant peak located at around 686.5 eV could be found in all spectra of the samples, attributed to F−C binding. In general, upon heating, with an increase in the carbonate content, the M−F/H−F ratio also increased.

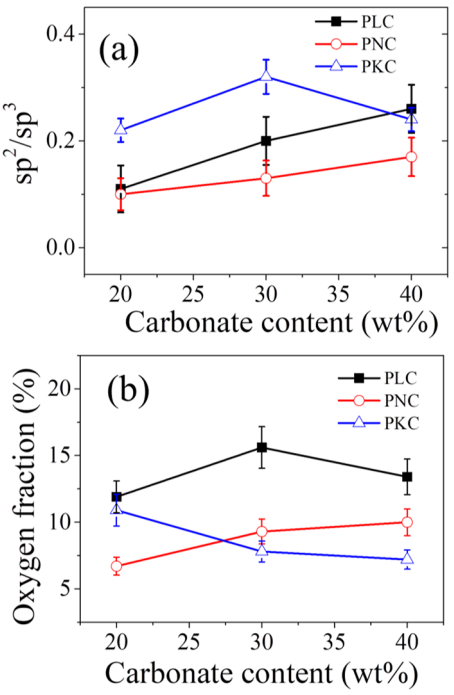


**Figure 4.** Variations of (a) $sp^2/sp^3$ and (b) O-related fraction with carbonate content for the investigated PLC, PNC, and PKC samples.

## 4. DISCUSSION

In a recent paper, we have reported the presence of a complex reaction loop in percolative composites PVDF/$K_2CO_3$ to gradually consume the raw materials.[6] After mixing the constituent phases, i.e., alkali metal carbonate ($M_2CO_3$, M = Li, Na, and K) and PVDF, in the presence of moisture, the composite samples before thermal treatment consisted of physically mixed PVDF and a certain amount of $MHCO_3$ as well as hydrated water in sesquihydrate or sesquicarbonate double salt systems because of moisture absorption.[4,7,19,20] Upon thermal treatment, decompositions of $MHCO_3$ and hydrated compound release water, and the generated water further reacts with $M_2CO_3$ to yield hydroxide due to the basic nature of $M_2CO_3$ (pH > 7):[21]

$$2MHCO_3 \rightarrow M_2CO_3 + H_2O + CO_2 \quad (1)$$

$$M_2CO_3{\cdot}nH_2O \rightarrow M_2CO_3 + nH_2O \rightarrow MOH + MHCO_3 \rightarrow \ldots \quad (2)$$

Although PVDF is inert and thermally stable up to 350 °C, having a relatively low melting point of around 177 °C,[22] in the presence of alkaline solutions, dehydrofluorination and structural alteration can easily occur at much lower temperatures.[23] In general, it is considered that PVDF dehydrofluorination occurs when OH attacks the hydrogen side, as the loss of hydrogen ions induces electron transfer to the F element causing it to leave the chain. Accordingly, the removal of HF results in the formation of a carbon−carbon double bond on the carbon chain,[24] or an $sp^2$ graphitic ring structure through cross-linking dehydrofluorination reactions of PVDF.[6,25]



https://doi.org/10.1021/acsomega.2c06857
ACS Omega 2023, 8, 14944−14951

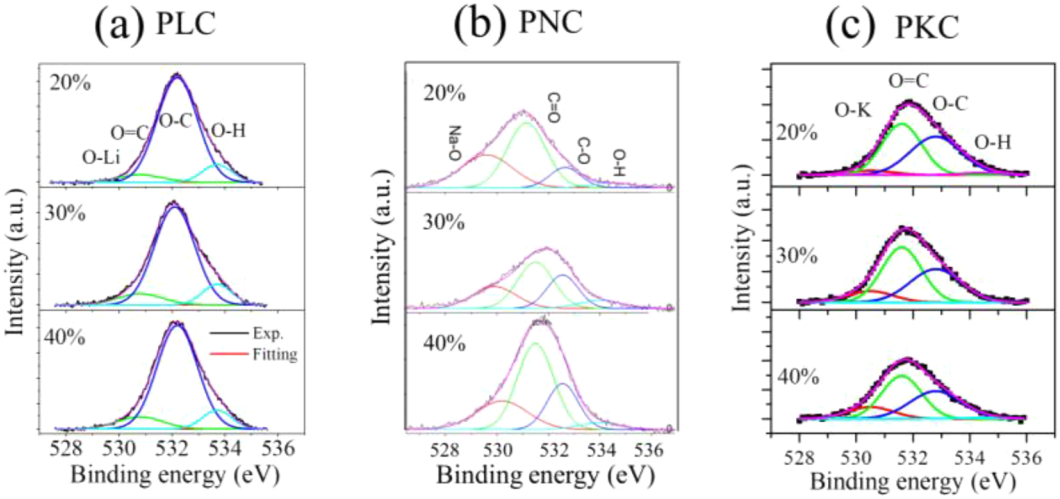


**Figure 5.** O 1s XPS spectra of the investigated (a) PLC, (b) PNC, and (c) PKC samples.

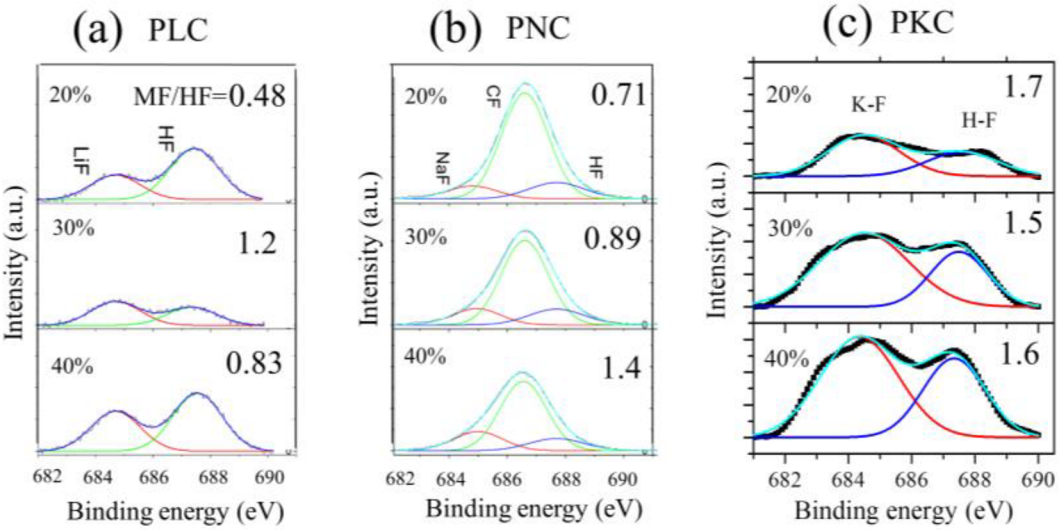


**Figure 6.** F 1s XPS spectra of the investigated (a) PLC, (b) PNC, and (c) PKC samples.

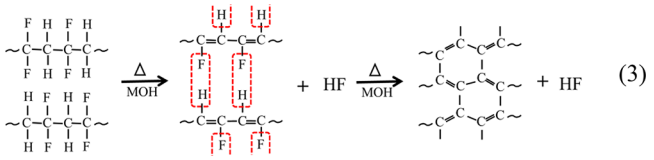


(3)

In this study, all PLC, PNC, and PKC samples exhibited both D and G peaks of activated carbon after thermal treatments (cf. Figure 1), indicating the effective occurrence of dehydrofluorination reactions during thermal treatments for the formation of $sp^2$ graphitic ring structures.[16] The insignificant change of Raman spectra of pure PVDF after thermal treatments at the same conditions confirmed that the generated carbon was not due to thermal decomposition/degradation of PVDF itself during heating.

The formation of HF following dehydrofluorination can react with the carbonate materials (as well as hydroxide and bicarbonate) to produce water and MF or $MHF_2$, showing a dependence on the content of $M_2CO_3$ in the raw mixture. The generation of $MHF_2$ in the final products could be confirmed by the appearance of new peaks in the X-ray diffraction analysis.[4] Accordingly, the produced water may disperse in the composite and further advance the dehydrofluorination reactions to modify the structure of the intermediate carbon product. It should be noted that the dehydrofluorination reactions in PVDF can be very complex in practice, since the reactions may result in the formation of different kinds of carbon products.

In the ideal cases of a formation of a pure $sp^2$ carbon ring structure (i.e., graphene or graphite, $C_{2n}$, cf. eq 3), the carbon products can be expected from the following two expressions:

$$n\mathrm{M_2CO_3} + 2(\mathrm{CH_2CF_2})_n \xrightarrow{\Delta} 2\mathrm{C}_{2n} + 2n\mathrm{MHF_2} + n\mathrm{CO_2} + n\mathrm{H_2O} \quad (4)$$

$$n\mathrm{M_2CO_3} + (\mathrm{CH_2CF_2})_n \xrightarrow{\Delta} \mathrm{C}_{2n} + 2n\mathrm{MF} + n\mathrm{CO_2} + n\mathrm{H_2O} \quad (5)$$

However, the final carbon product in practice (referred to as activated carbon) might not be the ideal $sp^2$ ring structure given in eqs 4 and 5, because of the presence of $sp^3$ carbon and the incorporation of H, F, and O atoms in the carbon structure, which may cause a distortion of the rings and induce a three-dimensional connection of carbon rings. In other words, the microstructure of the generated AC should depend on the practical process of PVDF dehydrofluorination. Indeed, as



https://doi.org/10.1021/acsomega.2c06857
ACS Omega 2023, 8, 14944−14951

shown in Figures 2 and 4, a significant difference in the ratios of $sp^2/sp^3$ and $I_D/I_G$ revealed distinct modifications of the AC structure by the type and content of added carbonate upon thermal treatments.

Such differences in activated carbon structures could be associated with the variation of actual process and degree of dehydrofluorination in the composites, induced by the change of the alkali metal ions and the resultant relevant properties of the materials.

First, because of the difference in the atomic mass of the alkali metal ions (Li < Na < K), for the cases of the same added weight percent of the carbonate materials, the mole percent of carbonate will be expected to decrease in the order PLC > PNC > PKC. In this study, even when 40 wt % lithium carbonate was added, the carbonate mole content was still smaller than the stoichiometric content required to fully consume the 60 wt % PVDF according to the chemical reactions of eqs 4 and 5. In other words, when a higher amount of carbonate is added in the reacting mixtures, the AC products may experience more dehydrofluorination reactions during thermal treatment, which corresponds to the formation of a higher fraction of $sp^2$ carbon. This seems able to explain the observed increase of $sp^2/sp^3$ and $I_D/I_G$ values with increasing carbonate content for the PLC and PNC samples (cf. Figures 2 and 4). However, it cannot explain why the values of $sp^2/sp^3$ and $I_D/I_G$ did not decrease in the order of PLC > PNC > PKC for the samples with the same weight percent; why the rates of increase for the two ratios with carbonate content were quite different for PLC and PNC; as well as why PKC showed an optimum value of carbonate content.

In practice, since smaller M ions correspond to higher mole percent of carbonate to approach the stoichiometric value, eqs 4 and 5 may compete, resulting in an increase of the ratio of MF/HF in the order of PLC < PNC < PKC for the same weight percent of carbonate (cf. Figure 6). The competition of the reactions can be confirmed by the results of F 1s XPS spectral analyses, since the production of MF and $MHF_2$ phases may cause a variation of the ratio of MF to HF. Considering the stoichiometric value (0.5) of MF/HF in $MHF_2$, a fraction of MF/HF > 0.5 leads to a preferential formation of MF, while a value smaller than it suggests the generation and adsorption of HF in the porous material. Note that the results of PVDF dehydrofluorination may cause the presence of an overwhelming majority of mesopores and macropores instead of micropores (<2 nm) and the formation of an interconnected pore system in the composite (cf. Figure S1). In general, increasing the carbonate content in the mixture seemed to result in an increase in MF/HF, i.e., preferential reactions of eq 5 rather than eq 4, except for the cases of PLC.

The exception might be associated with the relatively high amount of incorporated oxygen content in the carbon structure of PLC (cf. Figure 4b). After PVDF dehydrofluorination with the formation of C═C double bonds, the resultant allyl fluorides are more susceptible to hydrolysis.[23] Accordingly, the fluorine in the —CH═CF— group can be replaced by the hydroxyl group to form —CH═C(OH)—, while the latter one can transform to carbonyl ═CH—C(═O)—.

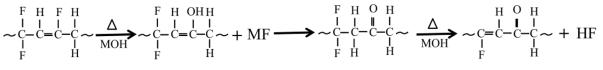


(6)

As a result, the oxygen content in the activated carbon exhibited an increase with an increase in the fraction of $sp^2$ carbon, as shown in Figure 4b. Note that oxygen incorporation into the carbon structural frame could both impede the formation of carbon rings and cause a distortion of neighboring carbon rings.[12] In other words, oxygen incorporation might cause a decrease of the $sp^2$ carbon fraction and influence the dehydrofluorination reaction, resulting in an alteration in the increase of the $sp^2/sp^3$ ratio.

With respect to PLC and PKC, the PNC samples after thermal treatments under the same conditions showed much smaller values of $I_D/I_G$ (Figure 2). This might be induced by the insufficient occurrence of dehydrofluorination reactions in PNC, which in turn can be confirmed by the presence of C—F and C—$F_2$ peaks in the C 1s XPS spectra (cf. Figure 3) and the appearance of a F—C binding-related peak in the F 1s spectra (cf. Figure 6b), as well as the existence of strong bands of C═O and O—M in the O 1s peak in PNC, but not in PLC and PKC (Figure 5).

As a result, the reactions were localized and constrained on the chain instead of wide-range cross-linking, which might cause the occurrence of other side reactions in the local regions in PNC, e.g.:

(i) The formation of a carbon−carbon triple bond (alkyne) owing to further dehydrofluorination of an alkene (F—C═C—H) group (cf. Figure 3)

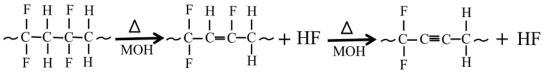


(7)

(ii) An irregular and discontinuous dehydrofluorination on the PVDF chains with parts of $CH_2$ and $CF_2$ remaining in the AC structure (cf. Figure 3)

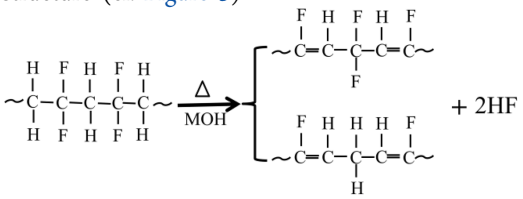


(8)

This may also cause a significant difference in the rate of increase of the $sp^2/sp^3$ ratio observed in the XPS analyses (Figure 4a). Note that, because of the presence of different side reactions, the reaction loop or the final product AC exhibited a strong dependence on the experimental conditions. For example, due to the formation of an $sp^2$ carbon chain and carbon ring, the fraction of $sp^2$ carbon in AC will increase along with the dehydrofluorination reaction proceeding until saturation. In the cases of PNC, the insufficient dehydrofluorination reactions could also be confirmed by increasing the thermal treatment time, which revealed an increase of the two ratios ($sp^2/sp^3$ and $I_D/I_G$) and a decrease of the Na−O fraction in the O 1s XPS spectra (cf. Figure S2).

The reasons for such kinds of distinct variations in the degree of PVDF dehydrofluorination for the investigated percolative composites might also be associated with the property of hygroscopy: for all present alkali metal carbonates, because of the strong affinity for water, hygroscopy can occur to attract moisture via either absorption or adsorption from the surrounding environment at room temperature if exposed to it, and alkali bicarbonate and hydrated alkali carbonate can be generated on the surfaces.[26] However, it should be noted that, in the case of hydrated sodium carbonate, efflorescence can occur for a loss of water with an impeded formation of $NaHCO_3$ in the raw mixture.[27] Accordingly, the reduced amount of generated water upon thermal treatments and the



https://doi.org/10.1021/acsomega.2c06857
ACS Omega 2023, 8, 14944−14951

inhibited formation of NaOH might cause insufficient dehydrofluorination reactions and the occurrence of the side reactions of eqs 7 and 8. Since carbon rings could not be generated by these reactions, a lower $I_D/I_G$ value and the remaining $CF_2$ on the carbon chains could be found. On the other hand, in the case of potassium carbonate, deliquescence can easily occur, which involves absorbing sufficient water to form an aqueous solution on the surface.[20] Accordingly, upon thermal treatments, more water will be involved to increase the efficiency of dehydrofluorination reactions. Indeed, we have newly confirmed that water plays a critical role on PVDF dehydrofluorination during thermal treatment.[7] Because of this higher efficiency of the dehydrofluorination process, PKC showed a marked increase in $I_D/I_G$ with the content of $K_2CO_3$ up to 30 wt %. However, further increasing the carbonate content above the percolation threshold may produce filler agglomerates, thus increasing the filler/filler interface population to the detriment of the matrix/filler interface fraction,[4] and result in an insufficient amount of HF, as well as a preferential reaction to form KF again. Consequently, during PVDF dehydrofluorination, the formation of KOH due to thermal decomposition and consumption of KOH due to competent reactions with HF might result in a complex dependence of the dehydrofluorination process on initial content of $K_2CO_3$.

Finally, the distinct ionic radius of the cation [Li (0.76 Å) < Na (1.02 Å) < K (1.38 Å)] may cause a difference in the thermal stability of alkali carbonate and bicarbonate materials. A smaller ionic radius results in a lower thermal decomposition temperature, since ionic nature increases on going down in a group due to the increase in the size of the cation.[28] Accordingly, the energy needed for the decomposition of $MHCO_3$ to start the dehydrofluorination reaction is in the order of PLC < PNC < PKC; i.e., it is easiest for the dehydrofluorination reactions to occur in PLC. Accordingly, the overall effect could result in a fast but relatively inefficient occurrence of PVDF dehydrofluorination in local regions of PLC with a relatively higher oxygen-related fraction, with respect to PKC.

As a result, the variation of $sp^2/sp^3$ ($I_D/I_G$) of the generated activated carbon showed a deviation from the order PKC < PNC < PLC. Note that $sp^2$ hybridizations play an important role in the electrical and electrochemical performance of carbon materials,[11,29,30] as the maximum $sp^2$ fraction or $sp^2/sp^3$ ratio at the optimal value of carbonate content seemed to be responsible for the best performance of the PKC film.[4] Indeed, for the investigated PLC, PNC, and PKC, similar trends in electrical conductivity fluctuations as those of $I_D/I_G$ could be observed (cf. Figure 7).

Exploring the transformation from insulator polymer-based mixtures to conductive carbon-based nanocomposites shows a new possible way to incorporate activated carbon in the polymer matrix to reach high flexibility of the system, which can also lower the manufacturing cost caused by adding expensive graphene/carbon nanotubes and/or reduce the stack and aggregation problems of graphene oxide and reduced graphene oxide for other carbon-based electrode materials.[31] In this study, we have shown that changing the carbonate source could significantly affect the AC structure, but a quantitative evaluation of the reactions is still a tough problem to be solved. The selectivity of the dehydrofluorination reactions (eqs 4−8) might be roughly estimated by analyzing the products for each competing reaction, although it is quite

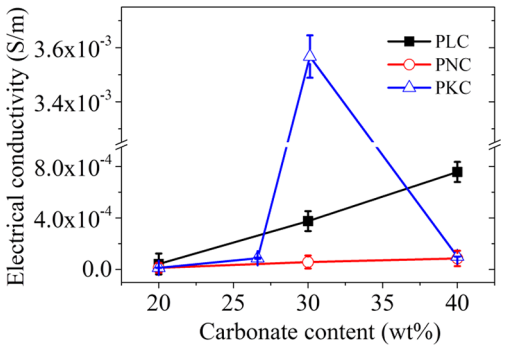


**Figure 7.** Variations of electrical conductivity (at $10^3$ Hz) as a function of carbonate content for the investigated PLC, PNC, and PKC samples.

hard to determine the component content. In general, estimation can be made based on the information retrieved from the chemical bonds and functional group content from the XPS and Raman analyses. The competition of main reactions to generate activated carbon (eqs 4 and 5) is mainly determined by the composition fractions and the hygroscopy property of the carbonate material. The side reaction to incorporate oxygen in the structure (eq 6) seems to be inevitable but could be associated with the reaction rate and the dehydrofluorination efficiency. The side reactions in eqs 7 and 8 appear to happen in local and constrained regions for the cases of insufficient dehydrofluorination reactions without wide-range cross-linking. The clarification of the mechanism of the formation of activated carbon can help to control the PVDF dehydrofluorination process for optimization of the material performance, as it has been demonstrated that a suitable variation of thermal treatment conditions can effectively modify the AC microstructure.

## 5. CONCLUSION

In this paper, structural variations of generated activated carbon, as induced by changing carbonate source and content in three different types of percolative composite systems fabricated from the mixtures of PVDF and different alkali metal carbonates [PVDF/$M_2CO_3$ (M = Li, Na, and K)], were investigated by Raman and X-ray photoelectron spectroscopies to clarify the effect of carbonate source on the process of PVDF dehydrofluorination under different experimental conditions. The results revealed a strong dependence of the AC structures on the type and content of the initial carbonate. Unlike PKC, which exhibited the presence of an optimal value of carbonate content with highest $sp^2$ fraction, both PLC and PNC showed an increase in $I_D/I_G$ and $sp^2/sp^3$ ratios with increasing carbonate content. PLC showed a complete consumption of the constituent carbonate components after thermal treatment, irrespective of their content ratios, while insufficient reactions were observed in PNC thermally treated under the same conditions, showing the presence of localized and constrained side reactions of dehydrofluorination with the appearance of an alkyne group and remaining C−F bindings. The significant variations of the AC structure in the three investigated systems were taken to be determined by practical dehydrofluorination reactions, associated with oxygen incorporation in AC and with the presence of side reactions. The origins of such variations might be related to their properties of hygroscopy, efflorescence, and deliquescence, as well as


https://doi.org/10.1021/acsomega.2c06857
ACS Omega 2023, 8, 14944−14951

thermal decomposition energy for $MHCO_3$ to start the dehydrofluorination reaction, induced by the difference in the alkaline metal ion of the carbonate sources. The clarification of the mechanism of dehydrofluorination reactions in this study could help to control the PVDF dehydrofluorination process for optimization of the material performance and provide the foundation for applications of the percolative composite to portable, flexible, and wearable energy storage systems.

## ■ ASSOCIATED CONTENT

### Data Availability Statement

All data generated or analyzed during this study are included in this published article and its Supporting Information file.

### Supporting Information

The Supporting Information is available free of charge at https://pubs.acs.org/doi/10.1021/acsomega.2c06857.

SEM image, absorption/desorption curves, and variations of $I_D/I_G$ and $sp^2/sp^3$ with carbonate content (PDF)

## ■ AUTHOR INFORMATION


### Corresponding Authors

**Wenliang Zhu** − *Ceramic Physics Laboratory, Kyoto Institute of Technology, 606-8585 Kyoto, Japan;* orcid.org/0000-0001-7532-9714; Email: wlzhu@kit.ac.jp

**Jiliang Zhu** − *College of Materials Science and Engineering, Sichuan University, Chengdu 610064, P. R. China;* orcid.org/0000-0002-2589-2477; Email: jlzhu167@scu.edu.cn

### Authors

**Kohei Okada** − *Ceramic Physics Laboratory, Kyoto Institute of Technology, 606-8585 Kyoto, Japan*

**Naoki Hoshida** − *Ceramic Physics Laboratory, Kyoto Institute of Technology, 606-8585 Kyoto, Japan*

**Yumi Yoshida** − *Molecular Chemistry and Engineering, Kyoto Institute of Technology, 606-8585 Kyoto, Japan*

**Alessandro Martucci** − *Dipartimento di Ingegneria Industriale, Università di Padova, 35131 Padova, Italy;* orcid.org/0000-0001-9601-8640

**Elia Marin** − *Ceramic Physics Laboratory, Kyoto Institute of Technology, 606-8585 Kyoto, Japan;* orcid.org/0000-0002-0981-7821

**Giuseppe Pezzotti** − *Ceramic Physics Laboratory, Kyoto Institute of Technology, 606-8585 Kyoto, Japan;* orcid.org/0000-0002-9663-2429

Complete contact information is available at: https://pubs.acs.org/10.1021/acsomega.2c06857


### Notes

The authors declare no competing financial interest.

## ■ ACKNOWLEDGMENTS

This work was supported by JSPS KAKENHI Grant Number JP21K04689.

## ■ REFERENCES


(1) Zhao, W.; Gong, J.; Wong, H. F.; Wang, Z.; Leung, C. W.; Ma, N.; Du, P. Percolative multi-susceptible PVDF/NZFO composite films with triply controlled high dielectric and magnetic properties. *J. Appl. Phys.* **2018**, *123*, 104104.

(2) Taha, T. A.; Mahmoud, M. H. Synthesis and characterization of PVDF-$Er_2O_3$ polymer nanocomposites for energy storage applications. *Mater. Chem. Phys.* **2021**, *270*, 124827.

(3) Horchidan, N.; Ciomaga, C. E.; Curecheriu, L. P.; Stoian, G.; Botea, M.; Florea, M.; Maraloiu, V. A.; Pintilie, L.; Tufescu, F. M.; Tiron, V.; Rotaru, A.; Mitoseriu, L. Increasing Permittivity and Mechanical Harvesting Response of PVDF-Based Flexible Composites by Using Ag Nanoparticles onto $BaTiO_3$ Nanofillers. *Nanomaterials* **2022**, *12*, 934.

(4) Wang, M.; Zhu, J.; Zhu, W.; Zhu, B.; Liu, J.; Zhu, X.; Pu, Y.; Sun, P.; Zeng, Z.; Li, X.; Yuan, D.; Zhu, S.; Pezzotti, G. The Formation of Percolative Composites with a High Dielectric Constant and High Conductivity. *Angew. Chem., Int. Ed.* **2012**, *51*, 9123−9127.

(5) Xu, P.; Fu, W.; Hu, Y.; Ding, Y. Effect of annealing treatment on crystalline and dielectric properties of PVDF/PEG-containing ionic liquid composites. *Compos. Sci. Technol.* **2018**, *158*, 1.

(6) Zhu, W.; Okada, K.; Li, Z.; Zhu, J.; Marin, E.; Pezzotti, G. Effect of component content variation on composition and structure of activated carbon in PVDF:$K_2$ $CO_3$. *Phys. Chem. Chem. Phys.* **2019**, *21*, 2382−2388.

(7) Zhu, W.; Hoshida, N.; Jati, G. N. P.; Yoshida, Y.; Adachi, K.; Zhu, J.; Ihara, M.; Marin, E.; Pezzotti, G. The role of water on dehydrofluorination in PVDF/$K_2CO_3$ percolative composites. *Materials Today Communications* **2022**, *32*, 103884.

(8) Chang, J.; Lin, Z.; Lin, M.; Zhu, C.; Zhang, J.; Wu, J. Solution processed F doped ZnO (ZnO:F) for thin film transistors and improved stability through co-doping with alkali metals. *J. Mater. Chem. C* **2015**, *3*, 1787−1793.

(9) Chen, G.; Liu, F.; Ling, Z.; Zhang, P.; Wei, B.; Zhu, W. Efficient Organic Light Emitting Diodes Using Solution-Processed Alkali Metal Carbonate Doped ZnO as Electron Injection Layer. *Front. Chem.* **2019**, *7*, 226.

(10) Zhang, L.; Zhan, X.; Cheng, Y. T.; Shirpour, M. Charge Transport in Electronic−Ionic Composites. *J. Phys. Chem. Lett.* **2017**, *8*, 5385−5389.

(11) Dwivedi, N.; Kumar, S.; Malik, H. K.; Govind; Rauthan, C. M. S.; Panwar, O. S. Correlation of $sp^3$ and $sp^2$ fraction of carbon with electrical, optical and nano-mechanical properties of argon-diluted diamond-like carbon films. *Appl. Surf. Sci.* **2011**, *257*, 6804−6810.

(12) Nakamura, M.; Takagawa, Y.; Miura, K.-i.; Kobata, J.; Zhu, W.; Nishiike, N.; Arao, K.; Marin, E.; Pezzotti, G. Structural alteration induced by substrate bias voltage variation in diamond-like carbon films fabricated by unbalanced magnetron sputtering. *Diamond & Related Materials* **2018**, *90*, 214−220.

(13) Zhu, W.; Arao, K.; Nakamura, M.; Takagawa, Y.; Miura, K.-i.; Kobata, J.; Marin, E.; Pezzotti, G. Raman spectroscopic studies of stress-induced structure alteration in diamond-like carbon films. *Diamond & Related Materials* **2019**, *94*, 1−7.

(14) Zhu, W.; Arao, K.; Marin, E.; Morita, T.; Nakamura, M.; Palmero, P.; Tulliani, J.-M.; Montanaro, L.; Pezzotti, G. Spectroscopic analyses of structural alterations in diamond-like carbon films deposited on zirconia substrates. *Diamond Relat. Mater.* **2022**, *124*, 108937.

(15) Barr, T. L.; Seal, S. Nature of the use of adventitious carbon as a binding energy standard. *J. Vac. Sci. Technol. A* **1995**, *13*, 1239.

(16) Ferrari, A. C.; Robertson, J. Interpretation of Raman spectra of disordered and amorphous carbon. *Phys. Rev. B* **2000**, *61*, 14095.

(17) Ferrari, A. C.; Robertson, J. Resonant Raman spectroscopy of disordered, amorphous, and diamondlike carbon. *Phys. Rev. B* **2001**, *64*, No. 075414.

(18) Liu, J.; Li, Z.; Jia, B.; Zhu, J.; Zhu, W.; Li, J.; Pan, H.; Zheng, B.; Chen, L.; Pezzotti, G.; Zhu, J. A freestanding hierarchically structured cathode enables high sulfur loading and energy density of flexible Li-S batteries. *Journal of Materials Chemistry A* **2020**, *8*, 6303−6310.

(19) Hill, A. E. Hydrated potassium sesquicarbonate, $K_2CO_3$·$2KHCO_3$·$3/2H_2O$. *J. Am. Chem. Soc.* **1930**, *52*, 3817−3825.

(20) Esat, K.; David, G.; Poulkas, T.; Shein, M.; Signorell, R. Phase transition dynamics of single optically trapped aqueous potassium carbonate particles. *Phys. Chem. Chem. Phys.* **2018**, *20*, 11598.

(21) Nakayama, F. S. Hydrolysis of sodium carbonate. *J. Chem. Educ.* **1970**, *47*, 67.
(22) Ouyang, Z.-W.; Chen, E.-C.; Wu, T.-M. Thermal Stability and Magnetic Properties of Polyvinylidene Fluoride/Magnetite Nanocomposites. *Materials* **2015**, *8*, 4553−4564.
(23) Brewis, D.M.; Mathieson, I.; Sutherland, I.; Cayless, R.A.; Dahm, R.H. Pretreatment of poly(vinyl fluoride) and poly(vinylidene fluoride) with potassium hydroxide. *Int. J. Adhesion and Adhesives* **1996**, *16*, 87−95.
(24) Ross, G. J.; Watts, J. F.; Hill, M. P.; Morrissey, P. Surface modification of poly(vinylidene fluoride) by alkaline treatment 1. The degradation mechanism. *Polymer* **2000**, *41*, 1685−1696.
(25) Rabuni, M. F.; Sulaiman, N. M. N.; Aroua, M. K.; Hashim, N. A. Effects of Alkaline Environments at Mild Conditions on the Stability of PVDF Membrane: An Experimental Study. *Ind. Eng. Chem. Res.* **2013**, *52*, 15874−15882.
(26) Yang, P.; Yang, H.; Wang, N.; Du, C.; Pang, S.; Zhang, Y. Hygroscopicity measurement of sodium carbonate, $\beta$-alanine and internally mixed $\beta$-alanine/$Na_2CO_3$ particles by ATR-FTIR. *Journal of Environmental Sciences* **2020**, *87*, 250.
(27) Zhou, S.; Zhou, S.; Zhang, J.; Tan, X.; Chen, D. Relationship between Moisture Transportation, Efflorescence and Structure Degradation in Fly Ash/Slag Geopolymer. *Materials* **2020**, *13*, 5550.
(28) Hartman, M.; Svoboda, K.; Čech, B.; Pohorely, M.; Šyc, M. Decomposition of Potassium Hydrogen Carbonate: Thermochemistry, Kinetics, and Textural Changes in Solids. *Ind. Eng. Chem. Res.* **2019**, *58*, 2868.
(29) Yuan, Q.; Lin, C.-T.; Chee, K. W. A. All-carbon devices based on sp2-on-sp3 configuration. *APL Materials* **2019**, *7*, No. 030901.
(30) Xie, Y.; Zhang, D.; Jati, G. N. P.; Yang, R.; Zhu, W.; Li, W.; Marin, E.; Pezzotti, G. Effect of structural and compositional alterations on the specific capacitance of hazelnut shell activated carbon. *Colloids Surf., A* **2021**, *625*, 126951.
(31) Li, Q.; Horn, M.; Wang, Y.; MacLeod, J.; Motta, N.; Liu, J. A Review of Supercapacitors Based on Graphene and Redox-Active Organic Materials. *Materials* **2019**, *12*, 703.


https://doi.org/10.1021/acsomega.2c06857
*ACS Omega* 2023, 8, 14944−14951